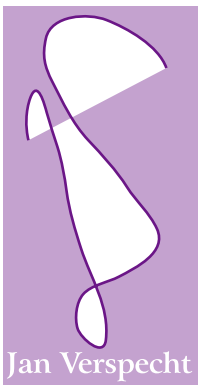

Jan Verspecht bvba

Gertrudeveld 15
1840 Steenhuffel
Belgium

email: contact@janverspecht.com
web: http://www.janverspecht.com

Linearization of Large-Signal Scattering Functions

Jan Verspecht, Dylan F. Williams, Dominique Schreurs,
Kate A. Remley, Michael D. McKinley

IEEE Transactions on Microwave Theory and Techniques, Vol. 53, No. 4, pp. 1369-1376

Linearization of Large-Signal Scattering Functions

Jan Verspecht, *Senior Member, IEEE*, Dylan F. Williams, *Fellow, IEEE*, Dominique Schreurs, *Senior Member, IEEE*, Kate A. Remley, *Member, IEEE*, and Michael D. McKinley, *Member, IEEE*

***Abstract*—We describe a linearization of large-signal scattering functions describing weakly nonlinear device behavior. The linearization takes on a convenient form similar to scattering parameters that clearly illustrates the role of phase-conjugated mixing products in the theory. We develop rules for the evolution of the linearization with time. We illustrate the theory with transistor measurements and apply the theory to the characterization of the reflection coefficients of a microwave source in its large-signal operating state.**

***Index Terms*—Frequency translation, large signal, network analysis, nonlinear, scattering parameters, vector signal generator.**

I. Introduction

REFERENCES [1] and [2] describe a linearization relating the large-signal forward and backward wave coefficients at the ports of a weakly nonlinear time-invariant device. By weakly nonlinear, we mean that the output signals of the device are a stable, single-valued, and continuous function of the input signals around the large-signal operating point and that the output signals only contain spectral components having frequencies which are linear combinations with integer coefficients of the frequencies present in the input signals. The linearization is used to describe nonlinear device behavior in terms of a large-signal steady-state operating point and a set of approximate linear relations between the real and imaginary parts of the small input and output signals superimposed on that operating point. In this study, we rewrite the linear relations described in [1] and [2] in a form similar to the conventional scattering-parameter matrices used to characterize the behavior of linear devices. This intuitive form clarifies the differences between conventional scattering parameters and the linearization we present here.

Perhaps the most successful and widely used linearization used to describe weakly nonlinear behavior in the microwave regime was developed by Torrey *et al.* [3] in 1948 to explain the electrical behavior of microwave mixers. Maas later summarized and expanded upon this theory in [4]. The theories of [3] and [4] explain the first-order behavior of microwave mixers with "conversion matrices" relating small frequency-domain voltages and currents or forward and backward wave coefficients at a set of discrete frequencies.

Manuscript received June 9, 2004; revised August 25, 2004.

J. Verspecht is with Jan Verspecht bvba, Londerzeel B-1840, Belgium (e-mail: contact@janverspecht.com).

D. F. Williams, K. A. Remley, and M. D. McKinley are with the National Institute of Standards and Technology, Boulder, CO 80305 USA (e-mail: dylan@boulder.nist.gov; dylan@ieee.org).

D. Schreurs is with the Department of Electronic Engineering, Katholieke Universiteit Leuven, B-3001 Leuven, Belguim (e-mail: dominique.schreurs@esat.kuleuven.ac.be).

Digital Object Identifier 10.1109/TMTT.2005.845771

More recently, [5]–[9] introduced "Hot" scattering parameters to describe the electrical behavior of weakly nonlinear devices and amplifiers operating under large-signal excitation. However, as we shall see later, the standard implementations of Hot scattering parameters fail to correctly describe the behavior of the phase-conjugated mixing products generated by even weakly nonlinear devices and amplifiers.[1]

Here we present a complete development of the theory described in [1] and [2] in terms of the Jacobian of a "large-signal scattering function." This Jacobian also finds use in harmonic-balance simulators [11]. We then rewrite that linearization in a form similar to the traditional scattering parameters used to describe linear circuits and devices, yielding an intuitive and useful description of the first-order nonlinear behavior of weakly nonlinear devices and circuits.

We also lift the restrictions of harmonically related frequencies and the special time reference employed in [1] and [2] and present general transformations between different time references, completing the theory.

Finally, we show that the theory encompasses the conversion-matrix approach for describing mixer behavior developed in [3] and [4] and includes the phase-conjugated mixing products missing from the Hot scattering-parameter description of [5]–[9]. We illustrate the theory with the characterization of a high electron-mobility transistor (HEMT) and the development of a new technique for measuring the reflection coefficients of a microwave source in its large-signal operating state. In both cases, we show the importance of capturing the phase-conjugation behavior of nonlinear devices in the linearization.

II. Large-Signal Scattering Functions

Reference [1] begins with a large-signal scattering function $\Im$ relating signals incident upon and reflected by a weakly nonlinear time-invariant device at a set of harmonic frequencies. We define the nonlinear large-signal scattering function $\Im$ somewhat more generally than in [1] by

$$\mathbf{B} = \Im(\mathbf{A}) \tag{1}$$

where $\mathbf{A}$ and $\mathbf{B}$ are vectors containing the wave coefficients of the large-signal incident (exciting) and reflected (response) waves at all of the ports of the device and at all of the frequencies present in the system. The frequencies in $\mathbf{A}$ and $\mathbf{B}$ may or may not be harmonically related, depending on the application. We also do not restrict the reference impedance of these wave

[1]Reference [10] recently introduced "large-signal scattering parameters." The large-signal scattering parameters $[S_J]$ of [10] are defined via $\mathbf{B} = [S_J]\mathbf{A}$, where $\mathbf{A}$ and $\mathbf{B}$ are vectors containing large-signal wave coefficients and do not correspond to any of the linearizations discussed here.

coefficients. However, we note that interpreting the wave coefficients and quantities derived from them is much more straightforward when they are set real [12].

We linearize (1) around a stable single-valued and continuous operating point of $\Im$ by writing $\mathbf{A}$ and $\mathbf{B}$ as $\mathbf{A} = \mathbf{A}_0 + \mathbf{a}$ and $\mathbf{B} = \mathbf{B}_0 + \mathbf{b}$, where $\mathbf{B}_0$ is the large-signal steady-state response to the large steady-state excitation $\mathbf{A}_0$, and $\mathbf{b}$ is the response to a small excitation signal $\mathbf{a}$ superimposed on $\mathbf{A}_0$.

When $\Im$ describes a linear time-invariant device, $\Im$ is analytic, and $\mathbf{A}$ and $\mathbf{B}$ can be related by a linear scattering-parameter matrix $[S]_{\text{linear}}$ via $\mathbf{B} = [S]_{\text{linear}}\mathbf{A}$. It then follows that $\mathbf{B}_0 = [S]_{\text{linear}}\mathbf{A}_0$ and $\mathbf{b} = [S]_{\text{linear}}\mathbf{a}$ as well. Furthermore, the elements of $[S]_{\text{linear}}$ relating wave coefficients at different frequencies vanish. This class of linear time-invariant electrical devices is very large and includes most passive microwave circuit elements. In addition, most active microwave transistors and amplifiers are designed to operate in a linear regime, and their electrical behavior can be described by a linear scattering-parameter matrix $[S]_{\text{linear}}$.

However, the scattering function $\Im$ describing the electrical behavior of a weakly nonlinear device is generally not analytic, so, even in the weakly nonlinear case, we cannot relate $\mathbf{A}$ and $\mathbf{B}$, or even $\mathbf{a}$ and $\mathbf{b}$, with linear scattering-parameter matrices. The inability of scattering parameters to approximate the response of weakly nonlinear circuits to even small excitation signals has been long appreciated in the computer-aided-design community [11].

Even so, when the elements of $\mathbf{a}$ and $\mathbf{b}$ are small, we can use the Jacobian $[J]$ of $\Im$ of a weakly nonlinear device evaluated at $\mathbf{A}_0$ and $\mathbf{B}_0$ to approximate the real and imaginary parts of the small response $\mathbf{b}$ to the real and imaginary parts of the small input signal $\mathbf{a}$.

Thus, for weakly nonlinear circuits, we can approximate $\mathbf{b}$ from $\mathbf{a}$ with

$$\begin{bmatrix} \operatorname{Re}(\mathbf{b}) \\ \operatorname{Im}(\mathbf{b}) \end{bmatrix} \approx [J] \begin{bmatrix} \operatorname{Re}(\mathbf{a}) \\ \operatorname{Im}(\mathbf{a}) \end{bmatrix} \equiv \begin{bmatrix} [J_{\text{RR}}] & [J_{\text{RI}}] \\ [J_{\text{IR}}] & [J_{\text{II}}] \end{bmatrix} \begin{bmatrix} \operatorname{Re}(\mathbf{a}) \\ \operatorname{Im}(\mathbf{a}) \end{bmatrix} \tag{2}$$

where $X = \operatorname{Re}(X) + j \operatorname{Im}(X)$ and the symbol $\approx$ indicates that this relation will hold approximately when all of the elements of $\mathbf{a}$ are small. Here, $[J]$ is a real Jacobian matrix formed from the first partial derivatives of the real and imaginary parts of $\mathbf{B}$ with respect to the real and imaginary parts of $\mathbf{A}$ evaluated at $\mathbf{A}_0$ and $\mathbf{B}_0$. Harmonic-balance simulators often use this Jacobian and Newton's method to iteratively solve nonlinear problems [11].

Defining $[S]$ and $[S']$ with

$$\begin{aligned} [S] &= 1/2([J_{\text{RR}}] + [J_{\text{II}}] + j([J_{\text{IR}}] - [J_{\text{RI}}])) \\ [S'] &= 1/2([J_{\text{RR}}] - [J_{\text{II}}] + j([J_{\text{IR}}] + [J_{\text{RI}}])) \end{aligned} \tag{3}$$

we can rewrite (2) as

$$\mathbf{b} \approx [S]\mathbf{a} + [S']\mathbf{a}^*. \tag{4}$$

The total response $\mathbf{B}$ can then be approximated as

$$\begin{aligned} \mathbf{B} &= \mathbf{B}_0 + \mathbf{b} \\ &= \Im(\mathbf{A}) \\ &= \Im(\mathbf{A}_0 + \mathbf{a}) \\ &\approx \Im(\mathbf{A}_0) + [S]\mathbf{a} + [S']\mathbf{a}^*. \end{aligned} \tag{5}$$

Equation (3) shows that there is a one-to-one correspondence between the complex elements of $[S]$ and $[S']$ and the real elements of the Jacobian matrix $[J]$ of $\Im$. Thus, we see that (4) is, in fact, a rather straightforward linearization of $\Im$ containing, as expected, the $(2n)^2$ real numbers of the Jacobian $[J]$, where n is the dimension of $\mathbf{a}$ and $\mathbf{b}$. The essential difference between the form of (2) and (4) is that (4) has been rearranged in terms of complex input and output vectors $\mathbf{a}$ and $\mathbf{b}$, rather than the real column vectors of (2).

Finally, for completeness, we note that we can write the matrices $[G]$ and $[H]$ defined in [1] by $\mathbf{b} = [G]\operatorname{Re}(\mathbf{a}) + [H]\operatorname{Im}(\mathbf{a})$ as $[G] = [S] + [S']$ and $[H] = j([S] - [S'])$.

It is perhaps best to think about the linearization as a pair of pairs. The first element of the pair is $\{\mathbf{A}_0, \mathbf{B}_0\}$, which describes the large-signal operating point at which the linearization was performed. $\mathbf{A}_0$ and $\mathbf{B}_0$ by themselves contain a wealth of information about the large-signal operating state of the weakly nonlinear device. The second element of the pair is the linearization described by $\{[S], [S']\}$. The matrices $[S]$ and $[S']$ describe how the device responds to additional small input signals superimposed on $\mathbf{A}_0$ and $\mathbf{B}_0$.

The matrix $[S]$ reduces to the small-signal scattering parameters $[S]_{\text{linear}}$ of a device when the device is linear and time invariant, and it relates elements of $\mathbf{b}$ directly to elements of $\mathbf{a}$. As the phase of an element in $\mathbf{a}$ increases, the corresponding phase of the elements in $\mathbf{b}$ will increase as well.

However, as a device enters its nonlinear regime of operation, the elements of $[S]$ relating different frequencies to each other will become nonzero. In addition, even weakly nonlinear devices usually create mixing products at both sum and difference frequencies of the input signals. Mixing products that include a difference frequency are particularly problematic, as increasing the phase or frequency of an input signal can result in a decrease in the phase or frequency of an output signal. This behavior will be described by the matrix $[S']$ in (4) and (5). This extra degree of freedom is required to complete the linearization, and it allows the linearization to apply to all first-order mixing products generated by a weakly nonlinear device.

Note that the matrix $[S']$, which relates elements of $\mathbf{b}$ to the *conjugate* of elements of $\mathbf{a}$, does not appear in the earlier efforts of [5]–[9] to develop a linearization capable of describing the electrical behavior of weakly nonlinear devices.

III. Translating the Time Reference

Reference [1] determines $[G]$ and $[H]$ with a time reference that sets to zero the phase of the component of $\mathbf{A}$ corresponding to the input signal at the fundamental frequency in the harmonic spectrum incident on the device. This choice of time reference simplifies the form of $\Im$, allowing it to be more easily measured with a large-signal network analyzer (LSNA).

However, this choice of time reference complicates the application of the theory when $\mathbf{A}_0$ contains several large signals at different input frequencies that are not harmonically related. For example, the steady-state large-signal operating point of a device could be determined by a signal with a number of tones at nearby frequencies that have no common fundamental frequency. This commonly occurs in two-tone distortion measurements.

Even when the signal that sets up the large-signal operating point of the device has a well-defined fundamental frequency,

choosing the time reference based on this fundamental frequency can still be problematic. For example, it becomes difficult to predict the effect of a small input signal at the fundamental frequency that is in quadrature with and superimposed upon the large fundamental component of the input signal. While the large signal at the fundamental often sets the operating point and time reference, applying a small signal in quadrature with the fundamental actually shifts that time reference. Furthermore, that time shift depends on the strength of the quadrature signal superimposed on the fundamental. Thus, the linearization as derived in [1] cannot predict the response to this quadrature signal without additional computations that take into account this shift of the time reference.

Here we choose a different approach. Rather than setting the time reference to the phase of one particular component of $\mathbf{A}_0$, we allow any choice of time reference and relate $\mathbf{A}_0, \mathbf{B}_0, [S]$, and $[S']$ at that time to those same quantities at any other time. This formalism simplifies the application of $[S]$ and $[S']$ and allows $[S]$ to reduce to the conventional scattering parameters of linear time-invariant devices in a natural way.

We can relate the complex frequency-domain vectors of wave coefficients $\mathbf{A}(t), \mathbf{B}(t), \mathbf{A}_0(t), \mathbf{B}_0(t), \mathbf{a}(t)$, and $\mathbf{b}(t)$ at time t to $\mathbf{A}(t_0), \mathbf{B}(t_0), \mathbf{A}_0(t_0), \mathbf{B}_0(t_0), \mathbf{a}(t_0)$, and $\mathbf{b}(t_0)$ at time t_0 with

$$\mathbf{X}(t) = e^{-j\mathbf{\Omega}(t-t_0)}\mathbf{X}(t_0) \tag{6}$$

where $\mathbf{X}$ in (6) can be replaced by any of $\mathbf{A}, \mathbf{B}, \mathbf{A}_0, \mathbf{B}_0, \mathbf{a}$, or $\mathbf{b}$, and $\mathbf{\Omega}$ is the diagonal matrix of angular frequencies of each of the elements of $\mathbf{X}$.

Using (6) and (1), we obtain the relation

$$\Im(\mathbf{A}(t)) = e^{-j\mathbf{\Omega}(t-t_0)}\Im(\mathbf{A}(t_0)). \tag{7}$$

Relation (7) is a direct consequence of the time invariance of the device and, therefore, of its large-signal scattering function $\Im$.

Using (6) and (4), we obtain

$$[S(t)] = e^{-j\mathbf{\Omega}(t-t_0)}[S(t_0)]e^{+j\mathbf{\Omega}(t-t_0)} \tag{8}$$

and

$$[S'(t)] = e^{-j\mathbf{\Omega}(t-t_0)}[S'(t_0)]e^{-j\mathbf{\Omega}(t-t_0)}. \tag{9}$$

The unexpected negative sign in the second exponent in (9) arises from the temporal behavior associated with the conjugate of $\mathbf{a}$ in (4).

These formulas allow $[S]$ and $[S']$ to be determined at a new time t once they have been determined at some specific time reference t_0. In practice, they allow us to characterize the device with one choice of time reference (typically, but not necessarily, with the phase of a fundamental input frequency set to zero), and then later use the characterization with any choice of time reference.

IV. Determining $[S]$ and $[S']$ at a Particular Operating State

Clearly, $[S]$ and $[S']$ determined at a particular large-signal state operating point $\mathbf{A}_0$ and $\mathbf{B}_0$ can be used to predict the performance of a weakly nonlinear device only when $|\mathbf{A} - \mathbf{A}_0| \ll |\mathbf{A}_0|$ and $|\mathbf{B} - \mathbf{B}_0| \ll |\mathbf{B}_0|$. The first step to predicting the performance of a weakly nonlinear device embedded in a circuit is to measure $[S]$ and $[S']$ at some particular $\mathbf{A}_0$ and $\mathbf{B}_0$ that we are able to create with our measurement instrumentation. In our numerical implementation, we determine $[S]$ and $[S']$ at a particular operating point $\mathbf{A}_0$ and $\mathbf{B}_0$ with linear least squares regression from large-signal data taken by an LSNA near $\mathbf{A}_0$ and $\mathbf{B}_0$, as described in the Appendix. This procedure is robust and easily programmed.

The actual large-signal operating state is often not known precisely beforehand. Thus, during device characterization, we must often measure $\mathbf{A}$ and $\mathbf{B}$ at a number of operating states and interpolate $[S]$ and $[S']$ over a space of operating points. The numerical implementation of the method described in [1] and [2] used artificial neural networks to interpolate $[S]$ and $[S']$ to the desired operating point from the set of operating points at which the device was measured. This allows additional flexibility in finding an $[S]$ and $[S']$ that best match the actual operating point of devices. For example, this procedure can be used to determine $[S]$ and $[S']$ at an operating point corresponding to an impedance-matched condition even though the measurement instrumentation is not perfectly matched.

V. Use of $[S]$ and $[S']$ to Predict Device Performance

The appearance of the matrix $[S']$ in (4) does not allow the usual formulas familiar to the microwave community to be employed for predicting the performance of a weakly nonlinear device when it is embedded in a larger circuit or system. Instead, a circuit simulator must be used to predict device performance. However, it is possible to develop fairly straightforward formulas for predicting the electrical behavior of a weakly nonlinear device embedded in a strictly linear time-invariant circuit or system containing sources.

Defining $[\mathbf{\Gamma}_s]$ as the diagonal matrix of reflection coefficients presented to the device by the linear external circuit in which it is embedded and $\mathbf{A}_s$ as the source amplitudes generated by the external circuit and incident on the device, then $\mathbf{A}, \mathbf{B}, [\mathbf{\Gamma}_s]$, and $\mathbf{A}_s$ must satisfy

$$\mathbf{A} = [\mathbf{\Gamma}_s]\mathbf{B} + \mathbf{A}_s. \tag{10}$$

This linear relation simply expresses the constraints imposed on $\mathbf{A}$ and $\mathbf{B}$ by the reflections $[\mathbf{\Gamma}_s]$ and sources $\mathbf{A}_s$ of the external circuit.

Substituting

$$\mathbf{B} \approx \mathbf{B}_0 + [S]\mathbf{a} + [S']\mathbf{a}^* \tag{11}$$

which is a direct consequence of (4) into (10), we obtain

$$([I] - [\mathbf{\Gamma}_s][S])\mathbf{a} - [\mathbf{\Gamma}_s][S']\mathbf{a}^* \approx \mathbf{A}_s - \mathbf{A}_0 + [\mathbf{\Gamma}_s]B_0 \tag{12}$$

where $[I]$ is the identity matrix. We can solve (12) directly by rewriting it in terms of its real and imaginary parts. This yields the linear matrix equation

$$\begin{bmatrix} \mathrm{Re}(1 - [\mathbf{\Gamma}_s][S] - [\mathbf{\Gamma}_s][S']) & -\mathrm{Im}(1 - [\mathbf{\Gamma}_s][S] + [\mathbf{\Gamma}_s][S']) \\ \mathrm{Im}(1 - [\mathbf{\Gamma}_s][S] - [\mathbf{\Gamma}_s][S']) & \mathrm{Re}(1 - [\mathbf{\Gamma}_s][S] + [\mathbf{\Gamma}_s][S']) \end{bmatrix} \times \begin{bmatrix} \mathrm{Re}(\mathbf{a}) \\ \mathrm{Im}(\mathbf{a}) \end{bmatrix} \approx \begin{bmatrix} \mathrm{Re}(\mathbf{A}_s - \mathbf{A}_0 + [\mathbf{\Gamma}_s]\mathbf{B}_0) \\ \mathrm{Im}(\mathbf{A}_s - \mathbf{A}_0 + [\mathbf{\Gamma}_s]\mathbf{B}_0) \end{bmatrix}. \tag{13}$$

We can now estimate $\mathbf{a}$ directly by solving (13) and thus predict the first-order behavior of the device when it is embedded in the external linear circuit.

VI. Role of $[S']$ in Mixer Characterization

We alluded previously to the crucial role that the matrix $[S']$ plays in representing the phase-conjugating behavior of mixing products generated by the vast majority of weakly nonlinear devices. In the following section, we will present some examples illustrating the role of $[S']$ in the theory. These examples show convincingly that both $[S]$ and $[S']$ are required to describe the response of weakly nonlinear devices to small excitations.

Mixers: Torrey *et al.* [3] introduced the notion of conversion matrices to describe the electrical behavior of diode mixers. Maas summarized the approach of Torrey *et al.* in [4] and defined an "S matrix," which we will call $[S^{\mathrm{M}}]$, from $[S^{\mathrm{M}}] \equiv (1+[Y_{\mathrm{n}}])^{-1}(1-[Y_{\mathrm{n}}])$, where $[Y_{\mathrm{n}}]$ is the diode's conversion (admittance) matrix.

Maas identifies port 0 with the mixer's IF port and port 1 with the mixer's RF port. In [4, eq. (4.87)], Maas describes the behavior of an RF mixer with

$$\begin{bmatrix} b_{\mathrm{IF}} \\ b_{\mathrm{RF}} \end{bmatrix} = \begin{bmatrix} S^{\mathrm{M}}_{00} & S^{\mathrm{M}}_{01} \\ S^{\mathrm{M}}_{10} & S^{\mathrm{M}}_{11} \end{bmatrix} \begin{bmatrix} a_{\mathrm{IF}} \\ a_{\mathrm{RF}} \end{bmatrix}. \tag{14}$$

In our notation, we can express (14) as

$$\mathbf{b} = \begin{bmatrix} b_{\mathrm{IF}} \\ b_{\mathrm{RF}} \\ b_{\mathrm{LO}} \end{bmatrix} \approx [S]\mathbf{a} = \begin{bmatrix} S^{\mathrm{M}}_{00} & S^{\mathrm{M}}_{01} & 0 \\ S^{\mathrm{M}}_{10} & S^{\mathrm{M}}_{11} & 0 \\ 0 & 0 & 0 \end{bmatrix} \begin{bmatrix} a_{\mathrm{IF}} \\ a_{\mathrm{RF}} \\ a_{\mathrm{LO}} \end{bmatrix} \tag{15}$$

where $[S'] = 0$.[2]

While increasing the phase of the signal at the IF port of an RF mixer increases the phase of the signal at the RF port of the mixer, it *decreases* the phase of the signal at the image (IM) frequency. Maas identified port -1 with the mixer's image port. Maas' equation [4, eq. (4.88)] describes the response of an image mixer to small input signals as

$$\begin{bmatrix} b^*_{\mathrm{IM}} \\ b_{\mathrm{IF}} \end{bmatrix} = \begin{bmatrix} S^{\mathrm{M}}_{-1,-1} & S^{\mathrm{M}}_{-1,0} \\ S^{\mathrm{M}}_{0,-1} & S^{\mathrm{M}}_{00} \end{bmatrix} \begin{bmatrix} a^*_{\mathrm{IM}} \\ a_{\mathrm{IF}} \end{bmatrix}. \tag{16}$$

In our notation, this is expressed as

$$[S] = \begin{bmatrix} S^{\mathrm{M}}_{00} & 0 & 0 \\ 0 & S^{\mathrm{M}*}_{-1,-1} & 0 \\ 0 & 0 & 0 \end{bmatrix} \quad [S'] = \begin{bmatrix} 0 & S^{\mathrm{M}}_{0,-1} & 0 \\ S^{\mathrm{M}*}_{-1,0} & 0 & 0 \\ 0 & 0 & 0 \end{bmatrix} \tag{17}$$

where we have defined $\mathbf{a}$ and $\mathbf{b}$ with $\mathbf{a} = [a_{\mathrm{IF}}, a_{\mathrm{IM}}, a_{\mathrm{LO}}]^{\mathrm{T}}$ and $\mathbf{b} =]b_{\mathrm{IF}}, b_{\mathrm{IM}}, b_{\mathrm{LO}}]^{\mathrm{T}}$, and where the superscript T indicates the transpose. Here, $[S']$ is required to describe the decrease of the phase of the image signal due to an increasing phase of input at the IF port. Similar relations have been developed by the computer-aided-design community relating the Jacobian $[J]$ to the conversion matrices of [3] and [4].

These relationships demonstrate the ability of the linearization discussed here to describe the basic electrical behavior of microwave mixers. In fact, the electrical behavior of any device that can be described by the conversion matrices of [3] and [4] can be equally well described by $[S]$ and $[S']$.

[2]The zeros in the last column of $[S]$ reflect the fact that the effect of changing either the amplitude or phase of a_{LO} has only a second-order effect on the signals at the IF and RF ports. While the effect of changing a_{LO} on the IF and RF signals is not available in this first-order linearization, we can use (8) to predict how $[S]$ will change as we change to a new time reference, which is equivalent to changing the phase of the local oscillator (LO).

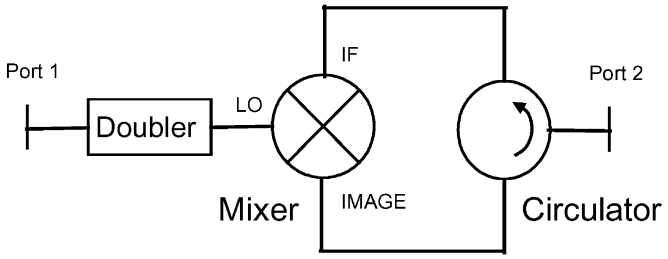

Fig. 1. Microwave phase conjugator. The frequencies at both ports of the phase conjugator must be the same. The frequency of the input signal at port 1 is doubled before being fed into the LO port of the mixer. The circulator routes the wave incident on port 2 to the IF port of the mixer, where it mixes with the doubled LO and generates an image signal at the same frequency. The image signal is then routed by the circulator back to port 2, where it appears as a reflected wave. Increasing the phase of the wave incident on port 2 decreases the phase of the reflected wave on port 2.

Phase Conjugator: Phase conjugators find use in optical telecommunication systems and as elements in reflective self-focusing antenna arrays [13]. Fig. 1 depicts a microwave phase conjugator. Port 2 of the microwave phase conjugator reflects a wave whose phase decreases as the phase of the signal incident on that port increases.

We can express the response of the ideal microwave phase conjugator of Fig. 1 to small input signals with

$$\begin{aligned} \mathbf{b} &= \begin{bmatrix} b_1 \\ b_2 \end{bmatrix} \\ &\approx [S]\mathbf{a} + [S']\mathbf{a}^* \\ &= \begin{bmatrix} s_{11} & 0 \\ 0 & 0 \end{bmatrix} \begin{bmatrix} a_1 \\ a_2 \end{bmatrix} + \begin{bmatrix} 0 & 0 \\ 0 & s_{22} \end{bmatrix} \begin{bmatrix} a^*_1 \\ a^*_2 \end{bmatrix}. \end{aligned} \tag{18}$$

Here again, $[S']$ is required to describe the decrease of the phase of the signal reflected by the phase conjugator when the phase of the incident wave increases.

VII. Transistor Characterization

Transistors and amplifiers typically generate harmonics and mixing products at their output when operated near saturation. Both $[S]$ and $[S']$ are required to characterize their performance in this regime.

To illustrate this, we tested an HEMT biased for maximum gain with a Hewlett-Packard LSNA set up in the conventional way and calibrated with the procedures outlined in [14]. We injected a 4-GHz sine wave into port 1 (the input) of the transistor and drove the transistor at power levels ranging from its small-signal regime far into saturation. We used this signal to derive our time reference for the measurements.

We simultaneously applied a small -24-dBm signal at the same frequency at the output of the transistor. The phases of this incident signal were uniformly distributed between 0° and 360°. We used this small signal incident on port 2 to determine S_{22} and S'_{22} with the procedure described in the Appendix. With a more complicated setup, we could have measured the other elements of $[S]$ and $[S']$.

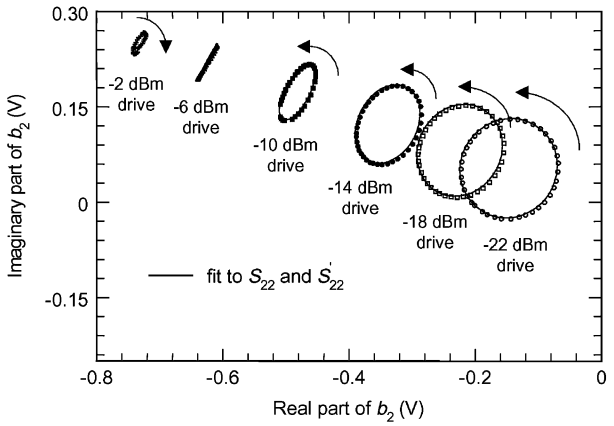

Fig. 2. Vector plots of the measured output wave coefficient b_2 as a function of the phase of the small-signal wave coefficient a_2 incident on an HEMT. The phase of a_2 is swept through 360° for a number of input drive levels. The markers indicate measured data. The arrows indicate the direction with which the phase of b_2 changes in response to an increase in the phase of a_2. The solid lines indicate the trajectories derived from the fit of S_{22} and S_{22}' to the measured data. If S_{22}' was zero, all of the trajectories would lie on circles and rotate in the counter-clockwise direction.

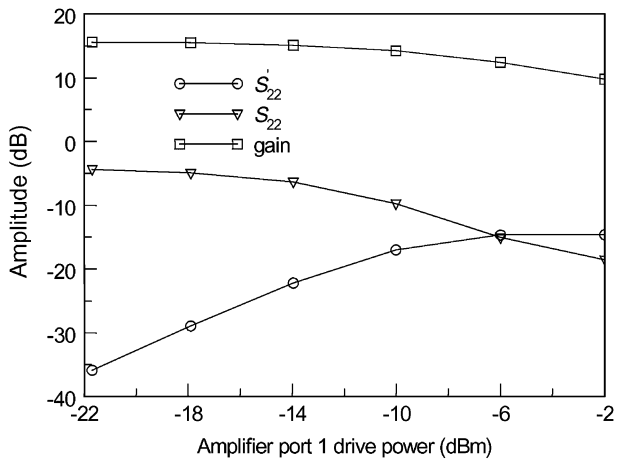

Fig. 3. Comparison of transistor gain, S_{22}, and S_{22}'. S_{22}' approaches 0 when the transistor operates in its small-signal regime, but becomes large and eventually exceeds S_{22} as the amplifier goes into saturation.

The symbols in Fig. 2 correspond to the complex outgoing wave coefficients b_2 we measured with the LSNA at the output of the transistor in response to the small -24-dBm incoming waves. These are plotted as a function of the drive power corresponding to the first element of $\mathbf{A}_0$ on port 1 at the input of the transistor. The solid lines in Fig. 2 show the fits we used to determine S_{22} and S_{22}' from the measured data. Sticking with convention, we set the reference impedance for the measurements to 50 Ω.

The arrows in the figure indicate the direction in which the phase of the outgoing wave coefficient b_2 changes as the phase of the wave coefficient a_2 incident on the output port of the transistor increases. At the lowest transistor drive levels, increasing the phase of a_2 increases the phase of b_2.

However, as the input drive power on port 1 is increased, the rate of increase in the phase of b_2 eventually stops and then reverses, as indicated by the arrows in the figure. This phase reversal is analogous to that of the phase conjugator of Fig. 1 and is due to the mixing of the second harmonic of the 4-GHz drive signal incident on port 1 generated by the transistor with the small signal incident on port 2 of the transistor. At high drive powers, this mixing generates a phase-conjugated mixing product at 4 GHz whose phase decreases when the phase of the incident signal is increased.

Note that, if S_{22}' was equal to zero, the trajectories in Fig. 2 would all lie on circles and rotate in the counterclockwise direction. Clearly, this would not explain the measured results correctly.

Fig. 3 compares the transistor's gain to the magnitude of S_{22} and S_{22}' as a function of the drive power at the transistor's input. Fig. 3 shows that the magnitude of S_{22}' decreases monotonically as the drive power on the transistor's input decreases. This figure also shows that the magnitude of S_{22}' increases as the amplifier enters saturation and eventually becomes larger than the magnitude of S_{22} as the drive power at the transistor's input exceeds

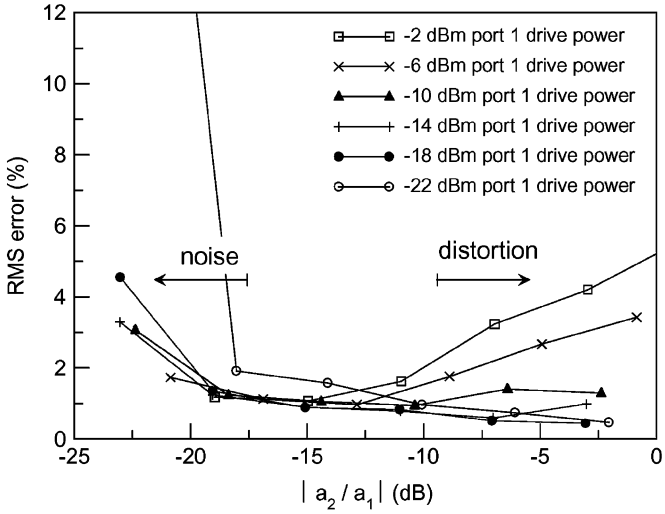

Fig. 4. RMS error in the predictions of the linearization as a function of the power of the small signal incident on port 2 of the transistor. Measurement noise raises the rms error at very low incident powers. As the power rises, the approximations begin to slowly degrade.

-6 dBm. At this point, the progression of the phases of b_2 in Fig. 2 reverses, as expected from (4).

We also briefly investigated the limits within which our linearization is valid for this particular device. We first measured S_{22} and S_{22}' with a small incident signal a_2 at the transistor's output. Then we plotted the rms differences of the actual b_2 we measured and the b_2 we predicted from S_{22} and S_{22}' in Fig. 4. The figure shows that our linearization is capable of predicting the transistor's response within a few percent when the incident signal a_2 on port 2 is much smaller than the drive signal a_1 on port 1, but begins to degrade when the incident power on port 2 approaches the drive power on port 1. This illustrates an important limitation of the linearization. While the linearization is useful for predicting the first-order behavior of weakly nonlinear devices in large-signal operation, it clearly cannot predict second-order effects that could be predicted by physical or other more complex circuit models.

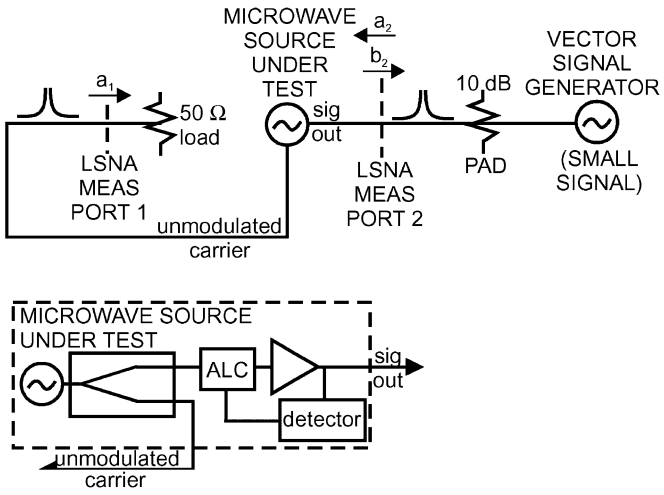

Fig. 5. Measurement configuration we used to measure the reflection coefficients Γ and Γ' of a microwave source with our LSNA. We turned the vector modulator in the source off for these experiments. The calibration reference planes are indicated by vertical dashed lines.

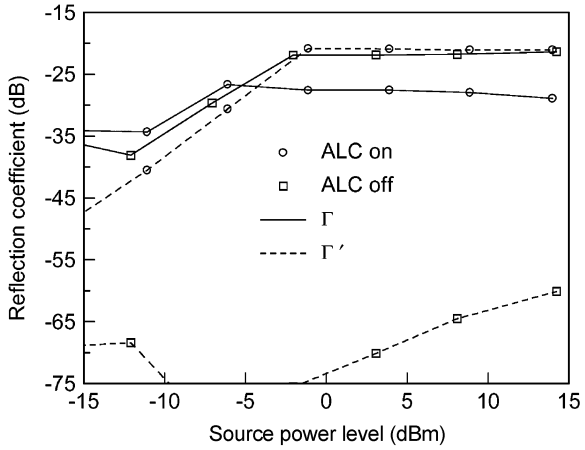

Fig. 6. Magnitudes of the reflection coefficients Γ and Γ' of our microwave source both with the ALC turned on and off.

VIII. Source Characterization

The reflection coefficients of microwave sources often vary with the power being generated by the source. Furthermore, it is difficult and often impossible to measure the reflection coefficient of microwave sources while they are operating with a conventional network analyzer.

Here, we show how our linearization can be used to characterize the small-signal reflection coefficients of microwave sources in their large-signal operating state. To illustrate, we calibrated an Agilent LSNA[3] to a 50-Ω reference impedance in the conventional way [14] at the two coaxial reference planes indicated by the vertical dashed lines in Fig. 5. We then used the LSNA to characterize a microwave source (in our case, a vector signal generator) at 2 GHz.

After calibrating the LSNA, we rearranged the measurement configuration as illustrated in Fig. 5. To establish an independent time reference for the measurements, we fed the signal from the unmodulated output port of the microwave source under test into the point at the rear of the couplers on port 1 of the LSNA where the LSNA's synthesizer is typically connected and terminated the measurement port 1 in a 50-Ω load. We used this signal to establish a common time reference for the measurements by setting to 0 the phase of a_1 measured by the LSNA at the reference plane on port 1 at 2 GHz. Note that we could not have used the output of the microwave source to establish a time reference for the measurements, as the phase of the source's output signal changes in response to small signals injected into its output during the characterization procedure.

We then connected the output of the microwave source under test to the second measurement port of the LSNA. We used the second vector signal generator to superimpose 40 small a_2 input signals on the large output signal b_2 generated by the microwave source under test. Each of these 40 small a_2 input signals had an amplitude about 10 dB below the large b_2 signal generated by the microwave source, had phases uniformly distributed between 0°–360°, and was at the same frequency as the b_2 signal generated by the source. We also could have used a fixed source slightly offset in frequency from the microwave source under test to generate these small a_2 input signals.

Finally, we used the LSNA measurements of a_2 and b_2 and the procedure described in the Appendix to determine the small-signal reflection coefficients Γ and Γ' (the S_{22} and S'_{22} we measure with the LSNA) of the microwave source under test with respect to the time reference we derived from the source's unmodulated output.

We measured Γ and Γ' with the microwave source's automatic level control (ALC) both turned on and turned off. The ALC monitors the signal level at the output of the microwave source and compensates dynamically for the detected variations.

Fig. 6 compares the magnitudes of Γ and Γ'. The figure shows that, with the ALC turned off, the source's conventional reflection coefficient Γ dominates. In this situation, one could use standard mismatch corrections to estimate the power delivered by the source to a load.

However, Fig. 6 also shows that, when the ALC is turned on, Γ' is significant and can even exceed Γ at higher output power levels. In essence, with the ALC on, the signal generator attempts to maintain a uniform output power even when illuminated by the small excitation signal a_2 from the second generator. This classic nonlinear limiting behavior gives rise to Γ'.

In fact, if the generator's ALC was able to exactly compensate for the reflected a_2 wave and maintain a perfectly constant output magnitude $|b_2|$, the trajectory of b_2 would be forced to lie on a short arc defined by a constant $|b_2|$. In this case, the magnitudes of Γ and Γ' would be equal. However, since the ALC cannot differentiate between the forward and backward waves incident on its sensor, it does an imperfect job of maintaining a constant output level. This gives rise to the difference in the magnitudes of the Γ and Γ' we measure when the ALC is on.

We note that, when Γ' is significant, we cannot describe its electrical behavior in terms of a Thévenin equivalent circuit, and we will not be able to use conventional mismatch corrections to

[3]The two LSNAs used in these experiments were prototypes, and were not assigned model numbers. We specified the manufacturer only to better define the experimental conditions. This does not constitute an endorsement by the National Institute of Standards and Technology. Other products may work as well or better.

determine the power that the source delivers to a load. Rather, we will have to use (13) for this purpose.

We also note that, once we have characterized the signal generator in this way, we can use (8) and (9) to translate the time reference for Γ and Γ' to some other convenient value. For example, we might choose a time for which the phase of the large output signal emanating from the generator is equal to 0.

IX. "Hot" Scattering Parameters

The "Hot" scattering parameters of [5]–[9] are also a linearization of the large-signal behavior of weakly nonlinear devices. However, the scattering parameters of [5]–[9] were not developed to handle the dependence of $\mathbf{b}$ on both $\mathbf{a}$ and $\mathbf{a}^*$, limiting their usefulness. For example, the scattering parameters of [5]–[9] cannot model outgoing waves from a device whose phases decrease when the phase of the coefficient of the incoming wave increases. Thus, they cannot model the electrical behavior of an image mixer, phase-conjugating circuits, transistors or amplifiers near saturation, or the electrical sources we characterized in this paper. Nevertheless, the scattering parameters of [5]–[9] can be considered to correspond to a submatrix of the scattering parameter matrix $[S]$ we describe here and represent a limited linearization of weakly nonlinear behavior.

X. Conclusion

We have presented a linearization of large-signal scattering functions that takes a form similar to that of the conventional scattering parameters used to describe linear circuits and devices. The representation we develop describes the response of weakly nonlinear devices to small excitations in a compact way. Furthermore, commercial LSNAs provide a convenient way of measuring the parameters describing the linearization.

In developing the theory, we avoided restrictions to harmonic signals and used a fixed, rather than an input-dependent, time reference for the linearization. We also showed that the linearization encompasses the conversion matrix approach commonly used to describe electrical mixers.

Finally, we illustrated the theory with several examples and with measurements of transistors and sources. All of these examples demonstrated the importance of the terms in the linearization describing the phase-conjugating behavior of nonlinear devices. While more study is certainly warranted, we also explored in a brief way some of the limitations of the linearization.

Appendix
Least Squares Fit of $[S]$ and $[S']$ From Measurement Data

In this study, we solved for individual elements of $[S]$ and $[S']$ one at a time with a classic linear least squares fit. The goal was to find $[S]$ and $[S']$ that best satisfy (5). An examination of (11) shows that, to find an approximation for S_{ij} and S'_{ij}, we must estimate the B_{0i}, S_{ij}, and S'_{ij} that best fit the

$$B_i \approx B_{0i} + S_{ij}a_j + S'_{ij}a_j^* \tag{19}$$

where B_i and B_{0i} are the ith elements of $\mathbf{B}$ and $\mathbf{B}_0$, respectively. Since (19) is linear in B_{0i}, S_{ij} and S'_{ij}, we can solve for B_{0i}, S_{ij}, and S'_{ij} with a linear least squares fit.

To do this, we performed a set of measurements of the large-signal responses B_{ik} of the device to different small-signal inputs a_{jk}. Here, the index k corresponds to measurement number, and each measurement is performed with different small-signal input a_{jk}.

To estimate S_{ij} and S'_{ij} from the data, we first arranged the small-signal input wave coefficients a_{jk} and large-signal responses B_{ik} into two vectors $\underline{\mathbf{a}}$ and $\underline{\mathbf{B}}$. We then constructed a matrix β whose first column was filled with ones, whose second column was equal to $\underline{\mathbf{a}}$, and whose third column was equal to $\underline{\mathbf{a}}^*$, the conjugate of $\underline{\mathbf{a}}$. Finally, we calculated the vector

$$s = (\beta^{\mathrm{H}} \cdot \beta)^{-1} \cdot (\beta^{\mathrm{H}} \cdot \underline{\mathbf{B}}) \tag{20}$$

where β^{H} is the Hermitian conjugate (the conjugate transpose) of β. The three elements of s are the least squares estimators of B_{0i}, S_{ij}, and S'_{ij}, respectively.

While it is known that this approach does not yield the best possible estimates in the presence of noise, it is extremely robust and easy to program. We also found that it offered very good estimates of $B_{0i,}S_{ij}$, and S'_{ij} for the highly over-determined data sets we used.

In our experiments, we held the magnitude of each a_{jk} constant while we varied the phase of each a_{jk} with k so that the small-signal inputs traced out a small circle in the complex plane. However, the approach is quite general. Not only can the method incorporate other data sets with no change in the procedure, but it is straightforward to simultaneously fit all of the elements of $[S]$ and $[S']$ when the measurement setup makes it difficult to control the small-signal excitation separately at each port and frequency.

Acknowledgment

The authors would like to thank S. Diddams, NIST, Boulder, CO, and M. Vanden Bossche, NMDG Engineering, Bornem, Belgium, for technical assistance with the measurements and D. Root, Agilent, Santa Rosa, CA, and J. Tauritz, University of Twente, Enschede Overijssel, The Netherlands, for their valuable suggestions and insights.

References

[1] J. Verspecht, M. Vanden Bossche, and F. Verbeyst, "Characterizing components under large signal excitation: Defining sensible 'large signal S-parameters'," in *49th ARFTG Conf. Dig.*, 1997, pp. 109–117.

[2] "Device for collecting measured data in signal port of DUT under various load conditions," U.S. Patent 2 003 057 963 pending, European patent JP2 003 194 861-2003-07-09 pending.

[3] H. C. Torrey and C. A. Whitmer, *Crystal Rectifiers*. New York: McGraw-Hill, 1948.

[4] S. Maas, *Microwave Mixers*. Boston, MA: Artech House, 1992.

[5] S. R. Mazumder and P. D. van der Puije, "Two-signal method of measuring the large signal S-parameters of transistors," *IEEE Trans. Microw. Theory Tech.*, vol. MTT-26, no. 6, pp. 417–420, Jun. 1978.

[6] G. Collinson and M. Jones, "A novel technique for measuring small signal S-parameters of an RF/microwave transistor, power amplifying stage for use in power amplifier stability analysis," in *IEEE MTT-S Int. Microwave Symp. Dig.*, Jun. 1993, pp. 1255–1258.

[7] J. Martens and P. Kapetanic, "Probe-tone S-parameter measurements," *IEEE Trans. Microw. Theory Tech.*, vol. 50, no. 9, pp. 2076–2082, Sep. 2002.

[8] T. Gasseling, D. Barataud, S. Mons, J. M. Nebus, J. P. Villotte, and R. A. Quere, "A new characterization technique of 'four hot S parameters' for the study of nonlinear parametric behaviors of microwave devices," in *IEEE MTT-S Int. Microwave Symp. Dig.*, vol. 3, Jun. 2003, pp. 1663–1666.

[9] T. Gasseling, D. Barataud, S. Mons, J. M. Nebus, J. P. Villotte, J. J. Obregon, and R. A. Quere, "Hot small-signal S-parameter measurements of power transistors operating under large-signal conditions in a load–pull environment for the study of nonlinear parametric interactions," *IEEE Trans. Microw. Theory Tech.*, vol. 52, no. 3, pp. 805–812, Mar. 2004.

[10] J. A. Jargon, K. C. Gupta, and D. C. DeGroot, "Nonlinear large-signal scattering parameters: Theory and application," in *63rd ARFTG Microwave Measurement Conf. Dig.*, Jun. 2004, pp. 157–174.

[11] V. Rizzoli and A. Neri, "State of the art and present trends in nonlinear microwave CAD techniques," *IEEE Trans. Microw. Theory Tech.*, vol. 36, no. 2, pp. 343–365, Feb. 1988.

[12] R. B. Marks and D. F. Williams, "A general waveguide circuit theory," *J. Res. Nat. Institute Standards Technol.*, vol. 97, no. 5, pp. 533–562, Sep.–Oct. 1992.

[13] Y. Chang, H. R. Fetterman, I. L. Newberg, and S. K. Panaretos, "Microwave phase conjugation using antenna arrays," *IEEE Trans. Microw. Theory Tech.*, vol. 46, no. 11, pp. 1910–1919, Nov. 1998.

[14] T. Van den Broeck and J. Verspecht, "Calibrated vectorial nonlinear-network analyzers," in *IEEE MTT-S Int. Microwave Symp. Dig.*, San Diego, CA, Jun. 1994, pp. 1069–1072.

Jan Verspecht (M'94–SM'05) was born in Merchtem, Belgium, on December 12, 1967. He received the electrical engineering and Ph.D. degrees from the Vrije Universiteit Brussel (VUB), Brussels, Belgium, in 1990 and 1995, respectively.

From 1990 to 1999, he was a Research Engineer with the Hewlett-Packard Company. From 1999 to 2002, he was a Technical Lead with Agilent Technologies. In 2003, he became Director and Chief Consultant with Jan Verspecht bvba, Londerzeel, Belgium. He has authored over 30 conference papers, 11 refereed publications, and the ARFTG short course on "Large-Signal Network Analysis." His research interests include the large-signal characterization and behavioral modeling of RF, microwave, and digital components.

Dr. Verspecht is a member of the Automatic RF Techniques Group (ARFTG). He was the recipient of the 2002 ARFTG Technology Award.

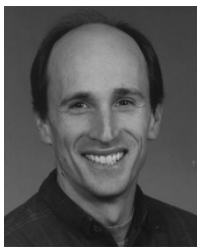

Dylan F. Williams (M'80–SM'90–F'02) received the Ph.D. degree in electrical engineering from the University of California at Berkeley, in 1986.

In 1989, he joined the Electromagnetic Fields Division, National Institute of Standards and Technology (NIST), Boulder, CO, where he develops metrology for the characterization of monolithic microwave integrated circuits (MMICs) and electronic interconnects. He has authored or coauthored over 80 technical papers.

Dr. Williams is an associate editor for the IEEE TRANSACTIONS ON MICROWAVE THEORY AND TECHNIQUES. He was the recipient of the Department of Commerce Bronze and Silver Medals, the Electrical Engineering Laboratory's Outstanding Paper Award, two Automatic RF Techniques Group (ARFTG) Best Paper Awards, the ARFTG Automated Measurements Technology Award, and the IEEE Morris E. Leeds Award.

Dominique Schreurs (S'90–M'97–SM'02) received the M.Sc. degree in electronic engineering and Ph.D. degree from the Katholieke Universiteit (K.U.) Leuven, Leuven, Belgium, in 1992 and 1997, respectively.

She is currently a Post-Doctoral Fellow of the Fund for Scientific Research–Flanders and a Visiting Assistant Professor at K.U. Leuven. She has been a Visiting Scientist with Agilent Technologies Inc., Eidgenössische Technische Hochschule (ETH) Zurich, and the National Institute of Standards and Technology (NIST). Her main research interest is the use of large-signal vector measurements for the characterization and modeling of nonlinear microwave devices.

Dr. Schreurs is vice-chair of the IEEE MTT-11 Committee on Microwave Measurements. She serves as workshop chair on the Executive Committee of the ARFTG.

Kate A. Remley (S'92–M'99) was born in Ann Arbor, MI, in 1959. She received the Ph.D. degree in electrical and computer engineering from Oregon State University, Corvallis, in 1999.

From 1983 to 1992, she was a Broadcast Engineer in Eugene, OR. From 1989 to 1991, she was Chief Engineer of an AM/FM broadcast station. In 1999, she joined the Radio-Frequency Technology Division, National Institute of Standards and Technology (NIST), Boulder, CO, as an Electronics Engineer. Her research activities focus on development of metrology for wireless systems, and characterizing the link between nonlinear circuits and system performance.

Dr. Remley was the recipient of the Department of Commerce Silver Medal and the Automatic RF Techniques Group (ARFTG) Best Paper Award.

Michael D. McKinley (S'94–M'96) was born in Kodiak, AK, on June 17, 1970. He received the B.S. (*cum laude*) in physical science from Biola University, La Mirada, CA, in 1994, the B.S.E.E. degree (*magna cum laude*) from Gonzaga University, Spokane, WA, in 1995, the M.S.E.E. degree from Northeastern University, Boston, MA in 2001, and is currently working toward the Ph.D. degree in electrical engineering at the Georgia Institute of Technology, Atlanta. He currently holds a temporary position with the National Institute of Standards and Technology (NIST), Boulder, CO.

From 1996 to 1998, he was a Hardware Design Engineer with the Intel Corporation, Hillsboro, OR. For most of 2000, he was an Intern with the Raytheon RF Components Group, Andover, MA. His current research interests include characterization and measurement of modulation schemes around 5 GHz.

Mr. McKinley is a member of Tau Beta Pi and Eta Kappa Nu. He was the recipient of the 1997 Intel Achievement Award for his work on high-speed motherboards.